A Fully Integrated 3.3–3.8-GHz Power Amplifier With Autotransformer Balun

Valentyn A. Solomko and Peter Weger

***Abstract*—This paper demonstrates the usage of a differential autotransformer as an output balun for an integrated power amplifier (PA) operating at low-gigahertz frequencies. In comparison with a conventional transformer balun, an autotransformer balun offers lower power losses, thereby increasing the saturated output power and reducing the gain compression at the edge of target power range. A theoretical analysis of an integrated autotransformer is given, comparison with a magnetic transformer is performed. The concept was experimentally verified in a fully integrated PA for a 3.3–3.8-GHz WiMAX band fabricated in SiGe : C bipolar technology. The active part of the amplifier implements the derivative superposition method aimed at linearizing the power transfer characteristic. Measured PA delivers saturated output power above 29 dBm. The maximum achieved power-added efficiency exceeds 40% at 3.4 GHz. At 3.5 GHz, 1-dB gain compression occurs for $P_{\rm out} = 24.6$ dBm.**

***Index Terms*—Autotransformer, balun, bipolar, derivative superposition, magnetic transformer, power amplifier (PA), WiMAX.**

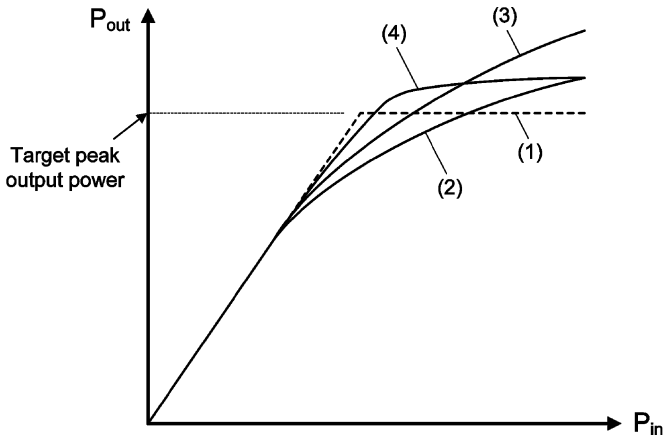

Fig. 1. Power transfer curves of: (1) ideal amplifier, (2) actual amplifier, (3) amplifier with increased saturated output power, and (4) amplifier employing derivative superposition technique.

I. Introduction

WiMAX technology based upon the IEEE 802.16 wireless MAN standard offers data rates of up to 75 Mb/s and coverage radius of about several miles. Achieving such high data rates while consuming moderate frequency bandwidth is only possible by employing high-order modulation schemes. This forces a power amplifier (PA) of WiMAX devices to meet strong linearity constraints. For mobile transmitter terminals where the supply voltage is often limited by 3.3 V, requirements on linearity become a bottleneck in PA design.

Several methods for improving linearity within the specified power range without significant degradation in gain and power-added efficiency (PAE) are known. Firstly, increasing the saturated output power helps to drive an amplifier into the more linear region of operation. In the case of limited supply voltage, this is accomplished by minimizing the mismatch and dissipative losses in passive output networks of the PA or by using a power-combining technique [1]. The die area and efficiency penalty of the last method limits its use in the designs for low-cost portable applications. Secondly, a derivative superposition technique [2] allows to improve linearity at the edge of target power range without evident drop in gain and PAE. Fig. 1 roughly illustrates the output characteristics of PAs employing the linearization techniques mentioned above. Among the other device-level methods is the analog predistortion technique [3]. The rest of the linearization techniques either require complicated analog or digital processing or are not applicable for the gigahertz range amplifiers [3].

A PA can be implemented either single ended or differentially (push–pull architecture). Single-ended realization has low tolerance to less than perfect RF ground inside the chip. Imperfect ground, which is caused by the parasitic inductance of bond wires, is a subject of unwanted output power drop and stability problems. Flip-chip packaging or low-inductive substrate contacting are required to minimize the effect of imperfect ground and improve the performance of a single-ended amplifier.

A differential structure is much less sensitive to the common mode ground inductance. This reduces the risk of oscillation and undesirable reduction in output power in the case when a bonding packaging technique is applied. A differential PA, however, requires an output balun, which is a subject of additional power losses when it is integrated on-chip.

This paper demonstrates the integrated differential PA employing two techniques aimed at reducing gain compression when driven with a large RF signal: autotransformer balun and two parallel-connected amplifiers biased to different operating points (derivative superposition method). A solid theoretical background on the use of an autotransformer balun is given in Sections II and III, and simulation results are presented. A derivative superposition method was extensively studied in the literature, thereby this paper focuses only on the implementation details for the specific structure.

Manuscript received March 27, 2009; revised June 25, 2009. First published August 11, 2009; current version published September 04, 2009.

The authors are with the Chair of Circuit Design, Brandenburg University of Technology Cottbus, D-03046 Cottbus, Germany (e-mail: Solomko.Valentyn@gmail.com; Peter.Weger@tu-cottbus.de).

Digital Object Identifier 10.1109/TMTT.2009.2027083

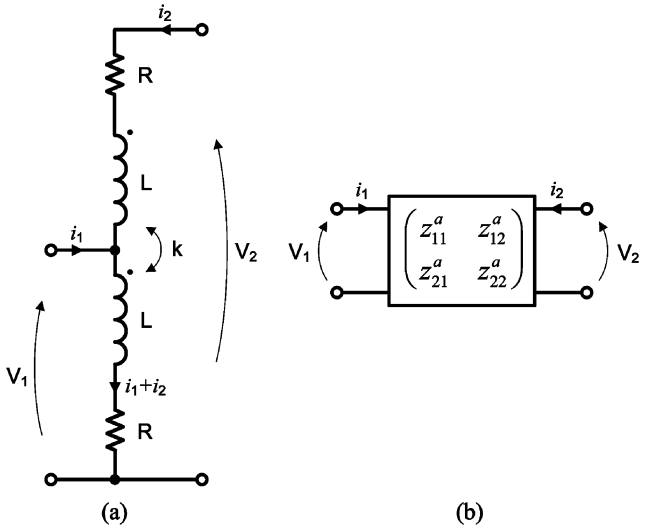

Fig. 2. (a) 1 : 2 autotransformer equivalent circuit. (b) Two-port network representation.

II. Power Losses in Transformers

This section presents the analysis of two single-ended transformers. The autotransformer balun considered further in this paper is based upon these two structures.

A. 1 : 2 Autotransformer With Losses

An autotransformer consists of a single coil tapped at some point. A center tapped autotransformer will be considered further. A simple lossy model of such a transformer is demonstrated in Fig. 2(a). Each half of the coil is modeled by a self-inductance L and a series resistance R. k represents a coupling factor between the two inductances, resulting in a mutual inductance of

$$M = k\sqrt{L \cdot L} = kL. \tag{1}$$

The left port is considered to give access to the primary winding of the autotransformer, which has an inductance of L. The inductance of the secondary winding is $2(L+M) = 2(1+k)L$. Thus, the impedance transformation ratio equals $L/\left(2(1+k)L\right) = 1/\left(2(1+k)\right)$.

For further analysis, the autotransformer is represented as a two-port network [see Fig. 2(b)], described as follows:

$$\begin{pmatrix} V_1 \\ V_2 \end{pmatrix} = \begin{pmatrix} z_{11}^a & z_{12}^a \\ z_{21}^a & z_{22}^a \end{pmatrix} \cdot \begin{pmatrix} i_1 \\ i_2 \end{pmatrix} \tag{2}$$

where

$$\begin{aligned} z_{11}^a &= j\omega L + R \\ z_{12}^a &= j\omega\left(L+M\right) + R \\ z_{21}^a &= j\omega\left(L+M\right) + R \\ z_{22}^a &= 2j\omega\left(L+M\right) + 2R. \end{aligned} \tag{3}$$

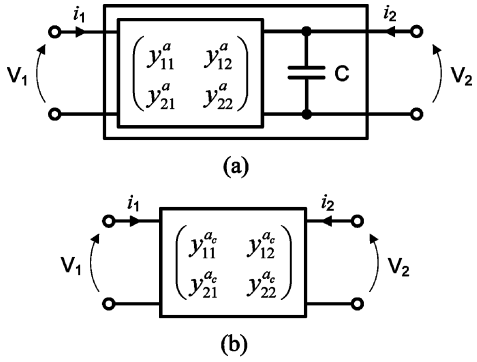

Fig. 3. (a) Tuned autotransformer. (b) y-parameter representation.

For the ease of representation after further addition of a parallel tuned capacitor, the z-matrix is transformed into the y-matrix

$$\begin{pmatrix} i_1 \\ i_2 \end{pmatrix} = \begin{pmatrix} y_{11}^a & y_{12}^a \\ y_{21}^a & y_{22}^a \end{pmatrix} \cdot \begin{pmatrix} V_1 \\ V_2 \end{pmatrix}. \tag{4}$$

Putting $\Delta_z = z_{11}^a z_{22}^a - z_{12}^a z_{21}^a$ and using (1), the elements of the admittance matrix expand out to

$$\begin{aligned} y_{11}^a &= \frac{z_{22}^a}{\Delta_z} = \frac{2}{j\omega L\left(1-k\right)+R} \\ y_{12}^a &= -\frac{z_{12}^a}{\Delta_z} = \frac{1}{j\omega L\left(1-k\right)+R} \\ y_{21}^a &= -\frac{z_{21}^a}{\Delta_z} = \frac{1}{j\omega L\left(1-k\right)+R} \\ y_{22}^a &= \frac{z_{11}^a}{\Delta_z} = \frac{j\omega L+R}{\omega^2 L^2\left(k^2-1\right)+2j\omega LR+R^2}. \end{aligned} \tag{5}$$

In order to keep the transformer in resonance, the capacitor C with the value

$$C = \frac{1}{\omega^2\left(2L+2M\right)} = \frac{1}{2\omega^2 L\left(1+k\right)} \tag{6}$$

is placed in parallel with the secondary winding. Fig. 3(a) indicates the resultant circuit.

The entire circuit is described by the following matrix equation:

$$\begin{pmatrix} i_1 \\ i_2 \end{pmatrix} = \begin{pmatrix} y_{11}^{a_c} & y_{12}^{a_c} \\ y_{21}^{a_c} & y_{22}^{a_c} \end{pmatrix} \cdot \begin{pmatrix} V_1 \\ V_2 \end{pmatrix} \tag{7}$$

where $y_{11}^{a_c} = y_{11}^a$, $y_{12}^{a_c} = y_{12}^a$, $y_{21}^{a_c} = y_{21}^a$, and $y_{22}^{a_c} = y_{22}^a + j\omega C$. In Fig. 3(b), the two-port network representation of the tuned autotransformer is given.

The obtained two-port network is now loaded with the admittance Y_L, as shown in Fig. 4. Assuming that $i_2/V_2 = Y_L$ and substituting it into (7), the admittance seen at the input is obtained as follows:

$$Y_{\text{in}} = \frac{i_1}{V_1} = y_{11}^{a_c} - \frac{y_{12}^{a_c} y_{21}^{a_c}}{y_{22}^{a_c} + Y_L}. \tag{8}$$

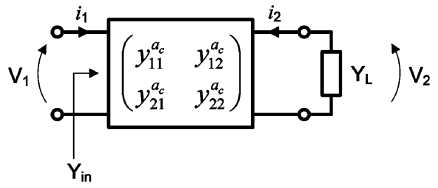

Fig. 4. Loaded autotransformer.

In general, Y_{in} in (8) can be represented as a function of circuit parameters and operating conditions as follows:

$$Y_{\text{in}} = f_a\left(\omega, Y_L, L, k, R\right). \tag{9}$$

The power delivered to the input of the tuned autotransformer and the power dissipated on the load are

$$P_{\text{in}} = \frac{1}{2}\left|V_1\right|^2 \cdot \Re\left\{Y_{\text{in}}\right\} \tag{10}$$

$$P_L = \frac{1}{2}\left|V_2\right|^2 \cdot \Re\left\{Y_L\right\}. \tag{11}$$

Consequently, the power loss in the network is defined as

$$P_{\text{loss}} = -10\log\frac{P_L}{P_{\text{in}}} = -10\log\frac{\left|V_2\right|^2 \cdot \Re\left\{Y_L\right\}}{\left|V_1\right|^2 \cdot \Re\left\{Y_{\text{in}}\right\}}. \tag{12}$$

From (7), it follows that

$$V_2 = \frac{V_1\left(Y_{\text{in}} - y_{11}^{a_c}\right)}{y_{12}^{a_c}}. \tag{13}$$

Substituting (13) and (8) into (12) results in

$$P_{\text{loss}} = -10\log\frac{\left|\dfrac{y_{21}^{a_c}}{y_{22}^{a_c}+Y_L}\right|^2 \cdot \Re\left\{Y_L\right\}}{\Re\left\{y_{11}^{a_c} - \dfrac{y_{12}^{a_c}y_{21}^{a_c}}{y_{22}^{a_c}+Y_L}\right\}}. \tag{14}$$

B. Magnetic Transformer With Losses

A magnetic transformer consists of two magnetically coupled coils (Fig. 5). In order to obtain the same impedance transformation ratio as in an autotransformer, the inductance of the secondary winding should be $L_s = 2(1+k)L$. Considering a circular geometry of the windings, one can write the following dependence of self-inductance and series resistance on the number of turns N [4]:

$$L_s \sim N^2 \quad R_s \sim N. \tag{15}$$

When inductance is scaled by a factor of $2(1+k)$ by means of increasing the number of turns, the series resistance is multiplied by a factor of $\sqrt{2(1+k)}$, resulting in $R_s = R\sqrt{2(1+k)}$.

Similar to the previous structure, the transformer is represented by the equation using an impedance matrix, namely,

$$\begin{pmatrix} V_1 \\ V_2 \end{pmatrix} = \begin{pmatrix} z_{11}^t & z_{12}^t \\ z_{21}^t & z_{22}^t \end{pmatrix} \cdot \begin{pmatrix} i_1 \\ i_2 \end{pmatrix}. \tag{16}$$

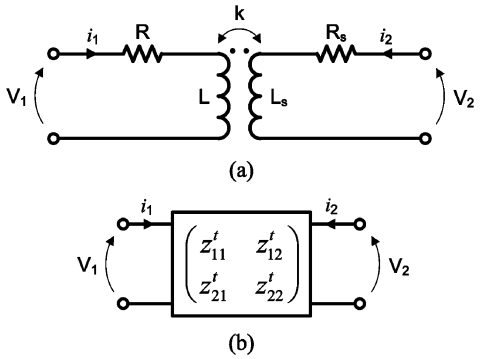

Fig. 5. (a) Equivalent circuit of a lossy magnetic transformer. (b) Two-port network representation.

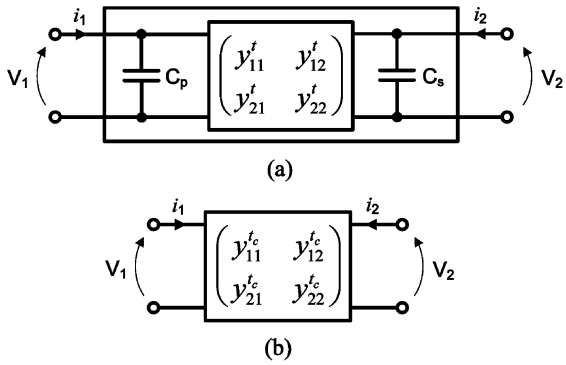

Fig. 6. (a) Double-tuned magnetic transformer. (b) y-parameter representation.

Expressing z-parameters through components values,

$$\begin{aligned} z_{11}^t &= j\omega L + R \\ z_{12}^t &= j\omega M \\ z_{21}^t &= j\omega M \\ z_{22}^t &= 2j\omega\left(1+k\right)L + R\sqrt{2\left(1+k\right)}. \end{aligned} \tag{17}$$

Here, $M = k\sqrt{L\cdot L_s} = k\cdot L\sqrt{2(1+k)}$. The elements of admittance matrix for the above-considered magnetic transformer are obtained as $y_{11}^t = z_{22}^t/\Delta_z$, $y_{12}^t = -z_{12}^t/\Delta_z$, $y_{21}^t = -z_{21}^t/\Delta_z$, and $y_{22}^t = z_{11}^t/\Delta_z$, where $\Delta_z = z_{11}^t z_{22}^t - z_{12}^t z_{21}^t$,

The transformer is double tuned to resonance by means of two capacitors [see Fig. 6(a)]

$$C_p = \frac{1}{\omega^2\left(L+M\right)} = \frac{1}{\omega^2 L\left(1+k\sqrt{2\left(1+k\right)}\right)} \tag{18}$$

$$\begin{aligned} C_s &= \frac{1}{\omega^2\left(2\left(1+k\right)L+M\right)} \\ &= \frac{1}{\omega^2 L\left(2\left(1+k\right)+k\sqrt{2\left(1+k\right)}\right)}. \end{aligned} \tag{19}$$

Together with the tuned capacitors, the transformer is described as follows [see Fig. 6(b)]:

$$\begin{pmatrix} i_1 \\ i_2 \end{pmatrix} = \begin{pmatrix} y_{11}^{t_c} & y_{12}^{t_c} \\ y_{21}^{t_c} & y_{22}^{t_c} \end{pmatrix} \cdot \begin{pmatrix} V_1 \\ V_2 \end{pmatrix} \tag{20}$$

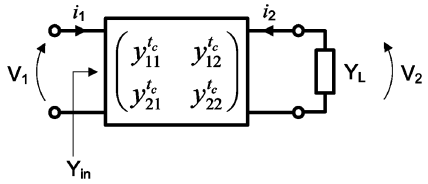

Fig. 7. Loaded magnetic transformer.

where $y_{11}^{t_c} = y_{11}^{t} + j\omega C_p$, $y_{12}^{t_c} = y_{12}^{t}$, $y_{21}^{t_c} = y_{21}^{t}$, and $y_{22}^{t_c} = y_{22}^{t} + j\omega C_s$.

The input admittance of the tuned transformer loaded by Y_L, as shown in Fig. 7, is

$$Y_{\text{in}} = \frac{i_1}{V_1} = y_{11}^{t_c} - \frac{y_{12}^{t_c} y_{21}^{t_c}}{y_{22}^{t_c} + Y_L}. \tag{21}$$

Finally, performing the same operations as for an autotransformer, the dissipative losses are obtained as follows:

$$P_{\text{loss}} = -10 \log \frac{\left| \dfrac{y_{21}^{t_c}}{y_{22}^{t_c} + Y_L} \right|^2 \cdot \Re\{Y_L\}}{\Re\left\{ y_{11}^{t_c} - \dfrac{y_{12}^{t_c} y_{21}^{t_c}}{y_{22}^{t_c} + Y_L} \right\}}. \tag{22}$$

In general, power losses defined by (14) and (22) are the functions of frequency, load admittance, and parameters of tuned transformer, namely, inductances, coupling factor, and parasitic resistances. The value of the tuning capacitor is already a function of L, k, and ω. When designing the PA, operating frequency and load admittance are defined by the specification and the designer is free to choose the transformer configuration. All parameters of the on-chip transformer strongly depend each on the other. In a transformer with fixed geometry, the series resistance of the windings and the coupling factor is proportional to the self-inductance of the windings. The diagrams in Fig. 8 demonstrate dissipative power losses in the magnetic transformer and autotransformer versus the coupling factor for two different values of primary inductance L and series resistance R. The diagrams are obtained using (14) and (22). The operating frequency is 3.5 GHz and the load impedance is 50 Ω (equivalently, $Y_L = 0.02$ S). If both transformers are laid out in a similar style and the number of turns in the primary winding is two or higher, it can be roughly assumed that the coupling factor in the transformer and autotransformer is approximately the same. Such an assumption is, however, invalid for one-turn structures.

According to Fig. 8, the autotransformer offers significantly lower power losses than the transformer. This is explained by the fact that, in autotransformer, the primary winding serves as a part of the secondary one, thereby reducing the total series resistance. It also demonstrates much weaker dependence of P_{loss} on the coupling factor value.

III. Autotransformer Balun

One can easily turn a magnetic transformer into balun by shorting the center point of the primary winding and the end

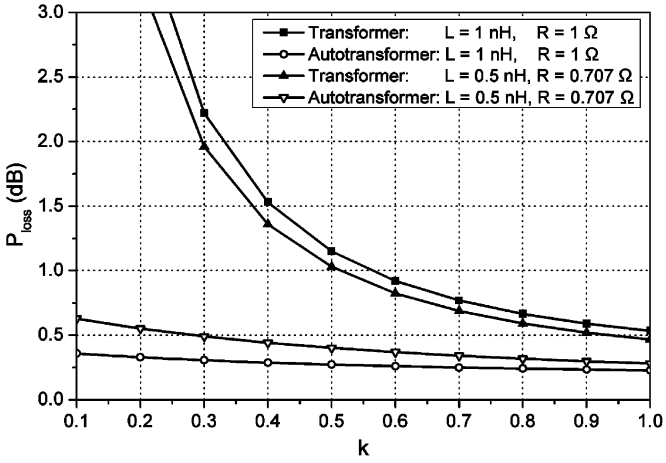

Fig. 8. Dissipative power losses in transformers.

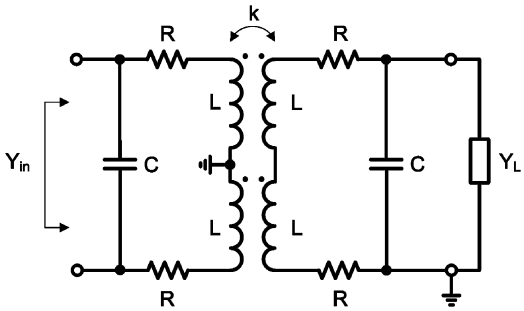

Fig. 9. Magnetic transformer balun.

terminal of the secondary winding to ac ground, as shown in Fig. 9. The tuning capacitor at differential input can equivalently be represented by two capacitors connected between each terminal of the input and ground. Each inductor L is magnetically coupled with the remaining three. The coupling factor k is the same for each inductor pair. When loaded by Y_L, the differential admittance seen at the input is given by

$$Y_{\text{in}} = f_t(\omega, Y_L, L, k, R) \tag{23}$$

where $f_t(\omega, Y_L, L, k, R)$ is a general form of the admittance transformation function.

As has been demonstrated in Section II, an autotransformer offers lower power losses than a magnetic transformer with the same impedance transformation ratio. Thus, it would be desirable to design a balun using an autotransformer. In contrast to a magnetic transformer, a differential autotransformer consists of just one common winding, which can be tapped to the ac ground only at one point. This applies strong restrictions on the use of an autotransformer as a differential to single-ended converter.

Fig. 10 indicates the structure of the autotransformer type balun. It consists of a single coil tapped at three points to form the terminals for differential input and ground. Each piece in between the tapped points and end terminals has the ohmic resistance R, the self-inductance L, and coupled with the remaining three pieces with coupling factor k. The center tap is connected to the ground. For convenience, we assume that the coil is divided in two parts: P and N (see Fig. 10). The load is connected

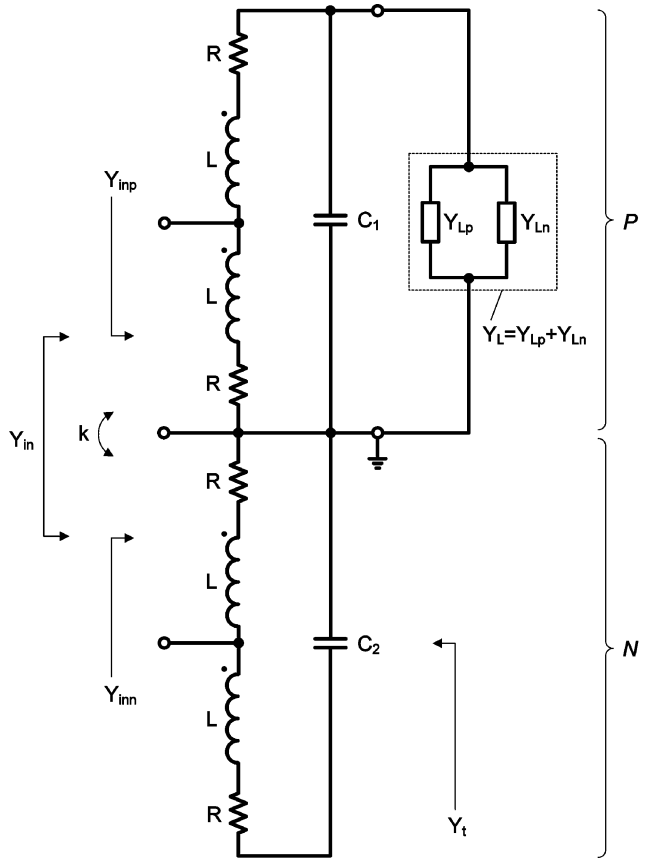

Fig. 10. Autotransformer balun.

to part P of the coil. Part N is galvanically decoupled from the load at ac.

The autotransformer balun can be derived from the structure shown in Fig. 9 by shorting the lower terminal of each winging to ground and applying the differential signal to the center taps of the coils. By taking this into consideration, the mechanism of the power transfer in the autotransformer balun becomes evident.

The differential signal consists of two phases balanced with respect to ground. One phase of the differential signal, which is connected to part P of the balun, couples into the single-ended output via the autotransformer, while the phase that is applied to part N is transferred to the output by means of magnetic coupling between parts P and N.

The dissipative losses in part P are caused by the losses in the autotransformer and are lower than in the magnetic transformer. The fraction of power transferred from part N to the load is defined by the losses in the magnetic transformer. Thus, if the differential input is properly matched, the structure in Fig. 10 offers lower power losses than the classical transformer type balun shown in Fig. 9.

The total number of turns seen by the differential input is equal to the number of turns at the load side. Consequently, the impedance transformation ratio of the ideal lossless autotransformer balun presented in Fig. 10 is $1:1$ (ideally implies that $k = 1$).

Important elements in the balun are the capacitors C_1 and C_2. They are used to drive the circuit into resonance. For now it is assumed that

$$C_1 = C_2 = \frac{1}{\omega^2 (2L + 6M)} = \frac{1}{2\omega^2 L (1 + 3k)}. \tag{24}$$

Consider a load admittance Y_L for the autotransformer balun consisting of two admittances connected in parallel, as shown in Fig. 10

$$Y_L = Y_{Lp} + Y_{Ln}. \tag{25}$$

The input admittance Y_{in} measured differentially is formed by the series connection of two admittances seen by each phase of the differential signal. The following relationship holds true:

$$\frac{1}{Y_{\text{in}}} = \frac{1}{Y_{\text{in}p}} + \frac{1}{Y_{\text{in}n}}. \tag{26}$$

Exact derivation of $Y_{\text{in}p}$ and $Y_{\text{in}n}$ can be performed by representing the balun with an n-port network and following the steps presented in Section II. Such an approach results in a complicated analytical expression for the input admittance, which does not clearly reflect the mechanism of load admittance transformation. We present a method for approximate derivation of the admittance seen at the differential input of the balun. The way in which $Y_{\text{in}p}$ and $Y_{\text{in}n}$ are estimated by means of this method clearly reproduces the physical processes in the demonstrated structure.

Part P and part N of the autotransformer balun will be considered independently. The standalone part P is nothing else but the single-ended autotransformer, exactly the same as shown in Fig. 2(a). The admittance $Y_{\text{in}p}$ can be expressed as follows:

$$Y_{\text{in}p} = f_a (\omega, Y_{Lp}, (1 + k) L, k, R) \tag{27}$$

where f_a is an admittance transformation function for a single-ended autotransformer expressed by (9). Note that the third argument of the function is $(1 + k) L$ rather than L. This happens because each piece L of the autotransformer balun is coupled magnetically with the other three pieces (but not one piece, as in the case of a single-ended autotransformer). In order to take into account the increase in total mutual inductance, we assume a single-ended structure, as if it had a self-inductance of each piece the factor of $1 + k$ higher.

Proceeding further with part N, we consider the admittance Y_t, which contributes to the $Y_{\text{in}n}$ part of the input differential admittance

$$Y_{\text{in}n} = f_a (\omega, Y_t, (1 + k) L, k, R). \tag{28}$$

The relationship between the load admittances of part P and part N is expressed through the admittance transformation function for the magnetic transformer (23), namely,

$$Y_t = f_t (\omega, Y_{Ln}, L, k, R). \tag{29}$$

Substituting (29) into (28) results in

$$Y_{\text{in}n} = f_a (\omega, f_t (\omega, Y_{Ln}, L, k, R), (1 + k) L, k, R). \tag{30}$$

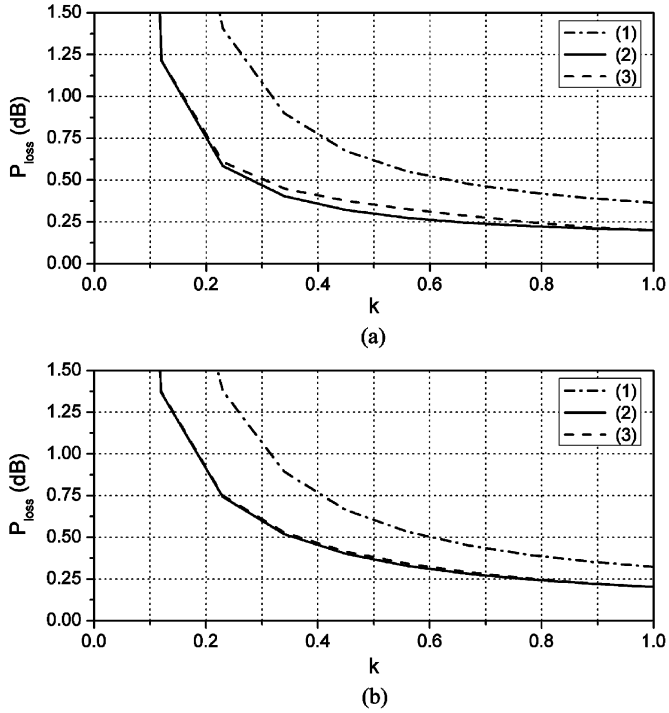

Fig. 11. Power losses in baluns at 3.5 GHz with $Y_L = 0.02$ S and (a) $L = 1$ nH, $R = 1\ \Omega$ and (b) $L = 0.5$ nH, $R = 0.707\ \Omega$. (1) Power losses in transformer balun. (2) Power losses in optimally matched autotransformer balun. (3) Power losses in autotransformer balun with source impedance complex conjugate matched with $Y_{\rm in}$ defined by (31).

The differential input admittance is derived from the following equation:

$$\frac{1}{Y_{\rm in}} = \frac{1}{f_a\left(\omega, Y_{Lp}, (1+k)\,L, k, R\right)} + \frac{1}{f_a\left(\omega, f_t\left(\omega, Y_{Ln}, L, k, R\right), (1+k)\,L, k, R\right)}. \quad (31)$$

Note that (31) is an approximate solution and some mismatch loss can happen when matching the source output impedance with (31). At this point, it would be instructive to compare power losses of the magnetic transformer balun and autotransformer balun shown in Figs. 9 and 10, respectively. For the case of an autotransformer, the following two different ways to match the input source impedance are considered.

- The input source impedance is complex conjugate matched with $Y_{\rm in}$, which is obtained using an exact analytical solution for the loaded autotransformer.
- The input source impedance is complex conjugate matched with $Y_{\rm in}$ defined by (31).

Fig. 11 demonstrates the calculated power losses over the coupling factor. The following two conclusions are drawn from the obtained curves.

- For the realistic values of the coupling factor $(0.5 < k < 0.8)$, theoretically predicted power losses in the autotransformer balun are approximately 0.25 dB below the losses in the magnetic transformer balun.
- $Y_{\rm in}$ obtained from (31) approximates the exact value of input admittance quite well.

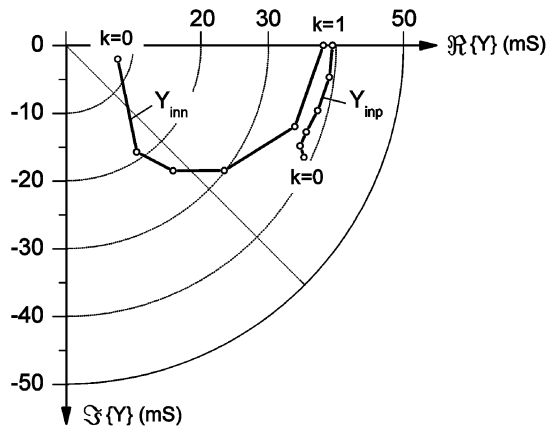

Fig. 12. Plot of $Y_{{\rm in}p}$ and $Y_{{\rm in}n}$ on a complex plane (3.5 GHz, $L = 1$ nH, $R = 1\ \Omega$).

Considering the differential autotransformer as the output network for an integrated PA, $Y_{{\rm in}p}$ and $Y_{{\rm in}n}$ must be equal in order to achieve such an improvement in power transfer. Indeed, two identical parts of the differential amplifier must be loaded by the same impedances to keep the symmetry and minimize mismatch losses and ground bounce inside the chip. $Y_{{\rm in}p}$ and $Y_{{\rm in}n}$ can be equal under some specific conditions, for example, when $R = 0$ and $k = 1$. Such conditions cannot be fulfilled in reality. Analysis proves that $Y_{{\rm in}p}$ and $Y_{{\rm in}n}$ are different for a finite value of series resistance and nonunity coupling factor. Complex admittances seen at the input of the differential autotransformer defined by (27) and (30) are plotted versus coupling factor in Fig. 12. Note that plotted admittances are an approximation rather than the exact solution. Two curves do not intersect each other. The minimum difference between $Y_{{\rm in}p}$ and $Y_{{\rm in}n}$ and, consequently, the best power transfer, can be achieved at the highest possible value of the coupling factor. Obviously, admittance $Y_{{\rm in}n}$ is much more sensitive to the change of the coupling factor than $Y_{{\rm in}p}$. This can be explained by the fact that the signal from part N (see Fig. 10) is transferred to the load mainly by means of the magnetic field. Thus, in order to minimize the difference between $Y_{{\rm in}p}$ and $Y_{{\rm in}n}$, the coupling factor between part N and part P should be maximized.

Capacitors C_1 and C_2 offer some degree of design freedom to tune the values of $Y_{{\rm in}p}$ and $Y_{{\rm in}n}$ for better matching. They can also compensate the inductive susceptance $(\Im\{Y\} < 0)$, which becomes dominant as the coupling factor is decreased. Up to now it was assumed that $C_1 = C_2$. In practice, the values of these capacitors should be different in order to compensate asymmetry and improve matching. Additional tuning capacitors can be added between the input terminals and the center tap.

When $Y_{{\rm in}p} \neq Y_{{\rm in}n}$, some asymmetry is introduced into the output stage of differential amplifier, which somewhat diminishes the advantages of the differential structure: a common mode bounce of the on-chip ground occurs, reducing the gain and output power. A risk of asymmetry seems to be the major disadvantage of this approach. Another drawback of the autotransformer balun is the presence of the dc path between the differential input and single-ended output, which makes necessary the use of bypass capacitors or center tapping the balun to ground and using a negative supply.

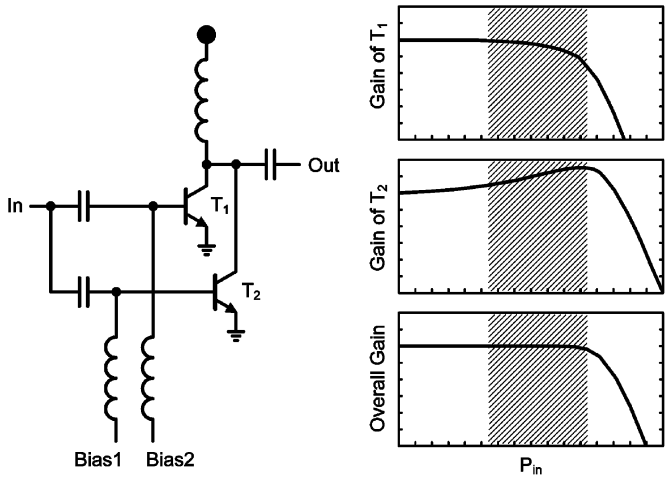

Fig. 13. Amplifier implementing derivative superposition technique.

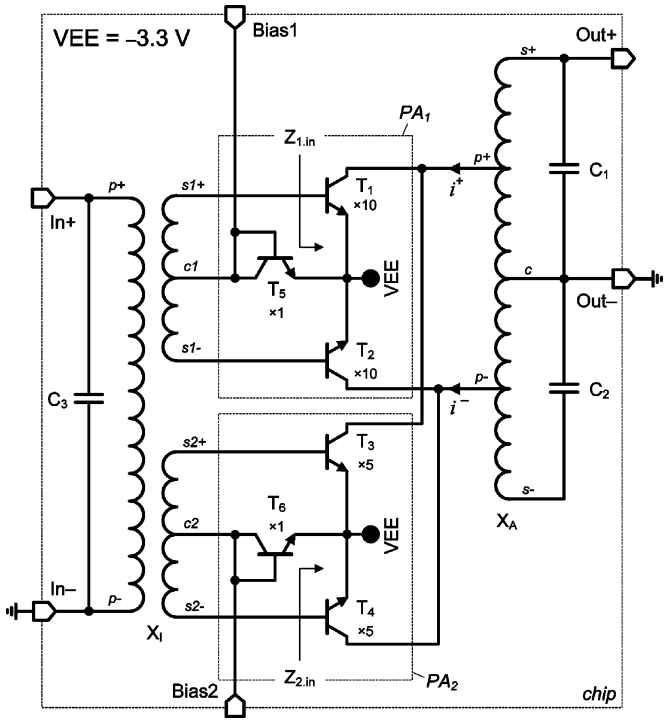

Fig. 14. Circuit diagram of the PA.

IV. Amplifier Design

A one-stage differential PA operating in the 3.3–3.8-GHz WiMAX band is designed and fabricated in Infineon SiGe : C bipolar technology with $f_T/f_{\max} = 33/55$ GHz. The amplifier incorporates two techniques to improve linearity: the derivative superposition technique employed in the active part [2] and the output autotransformer balun. The latter, as has been shown in Section III, is able to reduce dissipative power losses and increase the saturated output power.

A. Active Part Design

The main idea of the derivative superposition technique is to use several properly scaled and biased transistors connected in parallel to linearize the power transfer characteristic. In this way, the coefficients of the polynomial transfer function of the amplifier are modified in such a manner that the linearity within the desired power range can be improved. This technique was successfully applied to both small-signal [2], [5] and nonlinear [6], [7] field-effect transistor (FET) amplifiers. In this study, the derivative superposition method is realized by means of bipolar devices. Fig. 13 illustrates a basic circuit suitable for implementing the derivative superposition technique. The sizes of transistors are different. The device T_1 is biased into class AB and exhibits a gain rolloff when driven into the weak and moderate nonlinear regime (shaded area in the plots). Transistor T_2 operates in class B or class AB with a conduction angle close to π. Class B amplifiers are known to demonstrate some gain expansion when they are driven with large RF signals. This occurs due to the self-biasing effect [8]. T_2 compensates for gain compression of T_1 by increased gain at the proper power region.

The derivative superposition technique is implemented in the amplifier presented in this study. The simplified circuit diagram of the PA is shown in Fig. 14. Its a differential structure in which the input RF signal is coupled by means of a transformer with two secondary windings. Compound power transistors T_1 and T_2 are formed by the parallel connection of ten transistor units. The number of transistor units in T_3 and T_4 is five. Thus, the emitter area of the T_1–T_2 pair is twice the area of the T_3–T_4 pair. For convenience, differential stages formed by T_1–T_2 and T_3–T_4 will be called PA_1 and PA_2, respectively. The total quiescent current (including the dc current through transistors T_5 and T_6) is 81 mA. The overall output current is equal to the sum of the output currents of PA_1 and PA_2.

When all the transistors are biased at the same operating point (in this case, the derivative superposition PA transforms into a conventional PA), 81 mA is uniformly distributed among all transistors in the circuit. Under such biasing conditions, the simulated input differential impedance of each pair at 3.5 GHz is $Z_{1.\mathrm{in}} = 0.9 - j5.27\ \Omega$ and $Z_{2.\mathrm{in}} = 2.5 - j10\ \Omega$ (see Fig. 14).

For improving linearity, PA_2 is biased into class AB with a conduction angle of 1.6π, while PA_1 operates almost in class B with a conduction angle of 1.04π (here "almost" means that the quiescent current of PA_1 is not zero, and according to formal definition [3], it operates in class AB). In this case, the total idle current of 81 mA is distributed in the following way: the current density per one transistor in T_3–T_4 is three times higher than the current density per one transistor in T_1–T_2. The reason for making peak amplifier PA_1 larger is twofold. Firstly, the size compensates the reduction in transconductance due to the lower bias current and helps to keep the output power at high drive levels comparable with the power delivered by PA_2. Secondly, the lower small-signal input conductance and capacitance per unit area is compensated by the increased transistor size. Thus, the input impedance disbalance is reduced, resulting in $Z_{1.\mathrm{in}} = 1 - j5.5\ \Omega$ and $Z_{2.\mathrm{in}} = 1.78 - j9.7\ \Omega$.

It is important to note, that optimum biasing for band edges differs from that for 3.5 GHz. This is caused by the impossibility of providing equal matching for the entire 3.3–3.8-GHz band.

The amplifier is supplied from a single -3.3-V voltage source. In the presented design, the collectors of power transistors are connected to dc ground, which at the same time serves as a common ground for measurement setup. The emitters are

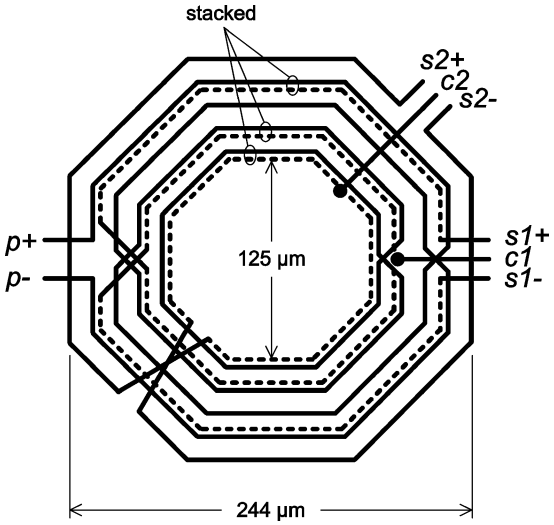

Fig. 15. Winding scheme of the input transformer X_I.

fed by -3.3 V. Due to the peculiarities of test board design, such a configuration of the supply network minimizes the bond-wire parasitics at the output of the amplifier.

B. Passive Structures Design

The technology used for amplifier fabrication offers five copper metal layers, four of which are thick and can be used for transformer design. Such a metallization stack allows to obtain high-quality structures with quite a complicated configuration. The technology features a low-conductive substrate, which helps to minimize power losses in the substrate.

The role of the input transformer X_I is to step down the source impedance, transform the input signal to a differential form, and divide it for applying to differential pairs PA_1 and PA_2. Since the PA incorporates no driver stage, its input impedance is very low. Thus, transformer X_I should provide a quite high impedance transformation ratio. Fig. 15 demonstrates the winding scheme of the input transformer. The number of turns in the primary winding is four, while the number of turns in each secondary winding is two. This results in impedance transformation ratio of $4:1$. The structure of transformer is quite complicated, incorporating in total eight turns. A stacked configuration was chosen to make the transformer compact and increase the coupling factor. Three turns marked with a dashed line are placed underneath the turns made of upper metallization layers. In spite of the increased interwinding parasitic capacitance typical for a stacked transformer, the resonant frequency is still above 3.8 GHz, which made it possible to use the design benefits of tuning capacitors. One-layer windings used in the structure do not cause any problems because no high current flows through the input transformer (this is not the case for output network, where the maximum current ratings protecting against electromigration become critical and limit the use of stacked structures). Each turn is 10-μm wide. The transformer is tuned to resonance by means of capacitor C_3 (see Fig. 14).

The key element of the presented amplifier is the output autotransformer X_A. Fig. 16 demonstrates its winding scheme. The autotransformer is designed in a symmetrical spiral style and incorporates six turns in total. All turns are 12-μm wide, except

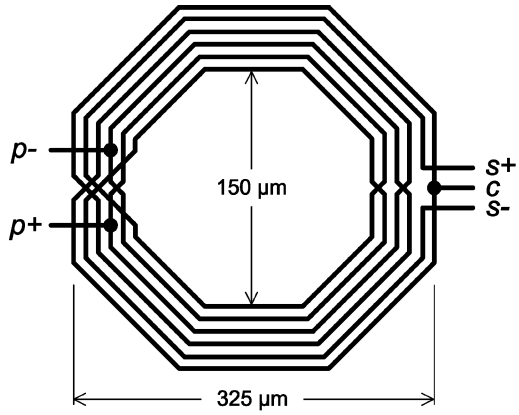

Fig. 16. Winding scheme of the output autotransformer X_A.

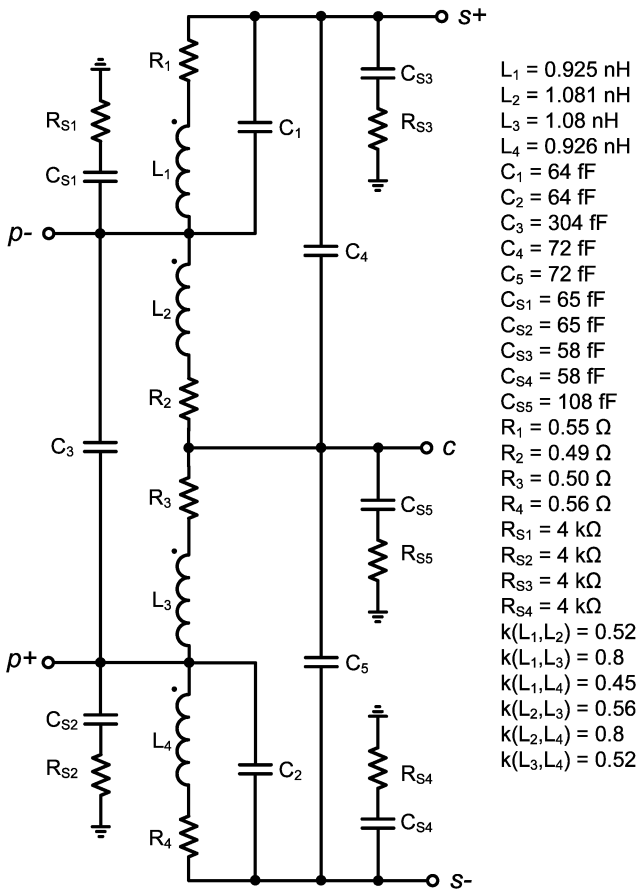

Fig. 17. Lumped-element model of the autotransformer X_A.

the outermost, which is 15-μm wide, and are spaced by the minimum design rule distance. Each turn is made of two uppermost metal layers connected in parallel. Such a configuration offers a good tradeoff between the interwinding capacitance, series resistance, and parasitic capacitance to the substrate.

In order to characterize the integrated differential autotransformer, its equivalent circuit was created (Fig. 17). The components values were extracted from the s-parameter model obtained after electromagnetic simulation. Inductances $L_1, \ldots, L_4$, resistances $R_1, \ldots, R_4$, and coupling factors $k(L_x, L_y)$ form the skeleton of the model, equivalent to the one shown in Fig. 10. In addition to these basic elements,

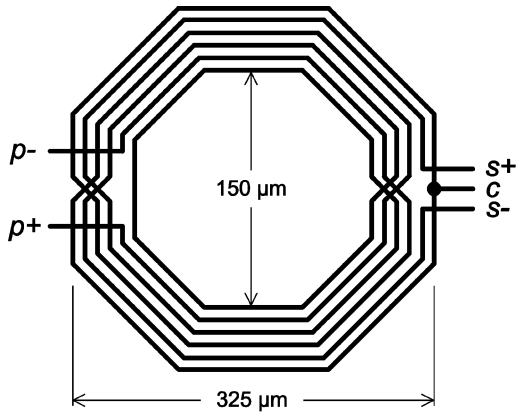

Fig. 18. Winding scheme of the magnetic transformer X_M.

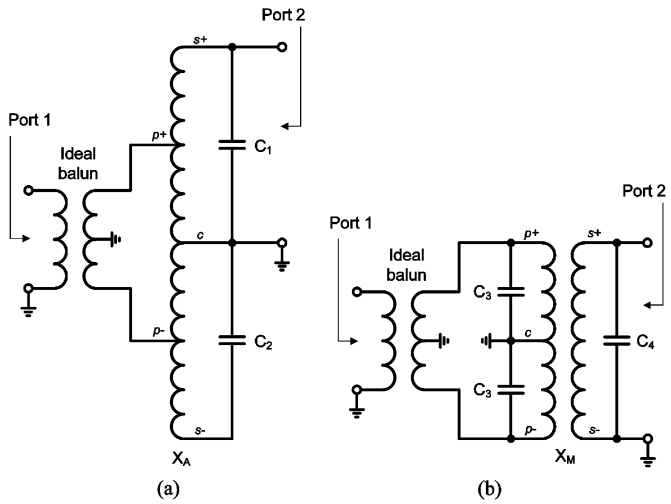

Fig. 19. Simulation setup for calculating dissipative power losses in: (a) autotransformer X_A and (b) magnetic transformer X_M.

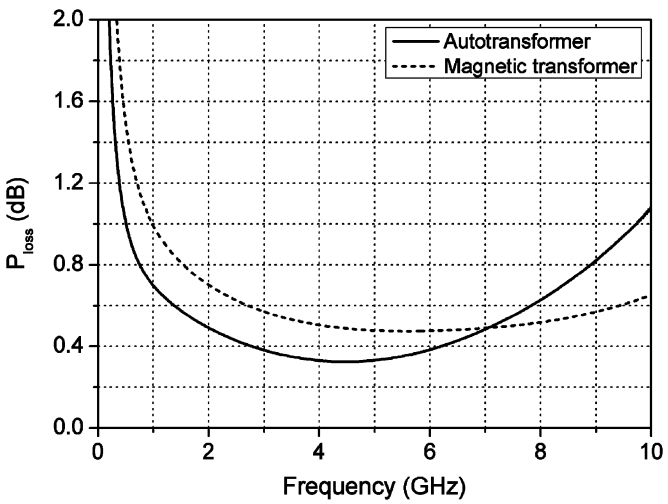

Fig. 20. Minimum dissipative power losses in autotransformer X_A and magnetic transformer X_M.

interwinding capacitances $C_1, \ldots, C_5$ and substrate parasitics are added. The latter are modeled by the resistances and capacitances with index s. The value of the resistances R_{sx} is pretty high, which makes the losses in the substrate material insignificant. Thus, the autotransformer model can be simplified without any significant degradation in accuracy by omitting substrate parasitics.

The number of turns in between every two adjacent terminals is 1.5, thereby the self-inductance of each piece is quite similar, close to 1 nH, and so is the series resistance. What makes this equivalent circuit differ from the conceptual model in Fig. 10 are the coupling factors. The deviation of $k(L_x, L_y)$ is quite significant, ranging from 0.45 to 0.8. Since the load is attached to the terminals $s+$ and c, the coupling between the inductance pairs L_3–L_4 and L_1–L_2 must be maximized. According to Fig. 16, windings of L_1 and L_3 are disposed next to each other along the entire turn, which results in a quite high coupling factor $k(L_1, L_3)$ of 0.8. The same is with L_2 and L_4. For the rest of the inductance pairs, the coupling is not so high because of the distributed structure of transformer windings and impossibility of providing the neighborhood for each winding pair.

The self-resonance estimated from the s-parameter model self-resonance frequency is 3.8 GHz. The values of tuning capacitors C_1 and C_2 were optimized to achieve the highest amplifier performance in terms of output power, efficiency, and linearity.

To validate the analytically stated superiority of the autotransformer balun in terms of dissipative power losses, a magnetic transformer was designed and compared with the autotransformer X_A. For convenience, the magnetic transformer is called X_M. To make the comparison relevant, the magnetic transformer was derived from X_A by changing the inter-winding connections. The inner and outer diameter, turns width, and metal structure of turns is identical to X_A. Fig. 18 illustrates the resultant winding scheme. The primary and secondary windings of X_M are wound in a complete alternate order to achieve maximum mutual magnetic coupling.

The mutual coupling extracted from the s-parameter model achieves a value of 0.8. The self-inductances of primary and secondary windings are 2.9 and 2.4 nH, respectively. The latter is almost four times lower than in X_A, causing the self-resonance for X_M to occur at 5.7 GHz.

For both the magnetic transformer and autotransformer, the dissipative power losses were estimated. Fig. 19 demonstrates the simulation setup used for s-parameters calculation. Since a push–pull PA drives the output transformer differentially, an ideal balun is placed at the input of each transformer. X_A and X_M are represented by their s-parameter models. Ideal tuning capacitors C_1–C_4 were included into the simulation setup. Note that all of them, except C_2, just alter the imaginary part of the transformer's admittance and do not influence the dissipative power losses. C_2, however, is connected inside the autotransformer balun and determines the amount of dissipated power. The value of C_2 is optimized to achieve the lowest loss at 3.5 GHz.

Fig. 20 shows the minimum dissipative power losses obtained from the simulated circuits presented in Fig. 19. The minimum losses are achieved only when the transformer is terminated by the pair of properly specified impedances and can be obtained from the simulated s-parameters of a circuit. The reader is referred to [9] for a detailed description of how to calculate the minimum dissipative power losses for a two-port network.

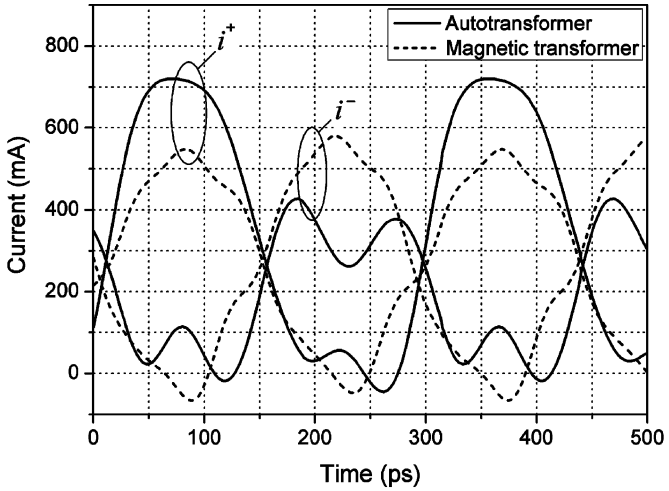

Fig. 21. Simulated collector currents of PAs with autotransformer X_A and magnetic transformer X_M for $P_{\rm in} = 20$ dBm.

The autotransformer offers 0.2-dB better performance in terms of power losses at low-gigahertz frequencies. With some performance penalties at 3.5 GHz, the losses can be decreased at frequencies above 7 GHz by tuning the capacitor C_2.

The curves in Fig. 20 are valid only for specific terminating impedances. In practice, however, the output impedance of a push–pull transistor pair and the load impedance will differ somewhat from the optimum value. We performed the simulation sweep of the load impedance at port 2 over a wide range: the real part was changing from 1 to 100 Ω, the imaginary part from −180 to 180 Ω. The impedance at port 1 was complex-conjugate matched to exclude mismatch losses. The curves showing the dissipative losses were observed over the 3.3–3.8-GHz frequency range. The autotransformer demonstrated lower losses than the magnetic transformer for any value of swept load impedance.

C. Simulation Results

The PA with an autotransformer balun was assembled and simulated in the ADS 2006 environment. For comparison, a version with magnetic output transformer X_M was designed. Terminals p+ and p− of the magnetic transformer were attached to the collectors of the power transistors, the supply voltage was applied to the center tap c. The transformer was tuned to resonance by means of capacitors C_3–C_4, as is shown in Fig. 19(b). The output of both PAs was matched to get the highest power and PAE.

Fig. 21 demonstrates the simulated collector current waveforms of the saturated amplifier (refer to Fig. 14 for location of currents i^+ and i^-). In the case of a magnetic output transformer, collector currents i^+ and i^- look symmetrical because it offers equal impedance for each phase of the differential signal. When the current reaches the maximum of 550 mA, the collector–emitter voltage of power transistors drops down to 0.24 V.

A different behavior is observed when an autotransformer is used as the output balun. Transistors T_1 and T_3 see lower impedance than T_2 and T_4, therefore producing 1.75 times larger current. The corresponding minimum collector–emitter voltage on T_1, T_3 and T_2, T_4 is 0.8 and 0.15 V, respectively. Simulation showed that despite nonoptimal matching, the PA with an autotransformer still delivers higher output power and PAE because of lower dissipative losses in the autotransformer balun.

TABLE I
SATURATED OUTPUT POWER VERSUS SUPPLY BOND-WIRE INDUCTANCE

L_{bond}	PA with autotransformer balun		PA with magnetic transformer balun	
	P_{out}, dBm	PAE, %	P_{out}, dBm	PAE, %
0.1 nH	28.84	47.4	28.53	43.4
0.2 nH	28.68	46.9	28.46	42.5
0.3 nH	28.55	46.5	28.41	42.5
0.4 nH	28.44	46.2	28.37	42.5

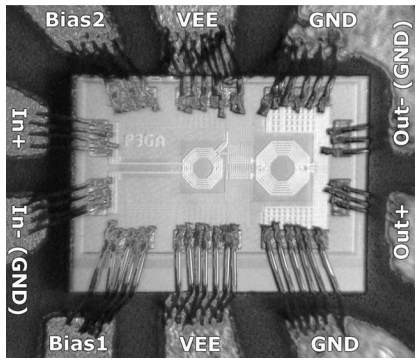

Fig. 22. Die photograph of the PA.

Asymmetrical collector current unavoidably results in a common mode bounce of on-chip ground with the input signal rate. The higher the inductance of supply bond wires, the stronger are the perturbations of on-chip ground and the more significant are the losses in output power and efficiency. Thereby the design was tested for the influence of bond-wire inductance on the saturated output power and PAE. Inductance $L_{\rm bond}$ was added in between the ports "VEE" and "Out-" of the amplifier (see Fig. 14) and terminals of a supply voltage source. For the case of a magnetic transformer balun, the inductance was connected between the center tap of transformer X_M and the supply source.

Table I summarizes the obtained output power and PAE for $P_{\rm in} = 20$ dBm. The PA with an autotransformer delivers higher output power and has better PAE. However, the dependence of $P_{\rm out}$ and PAE on the value of bond-wire inductance is stronger—the power drop is approximately −0.13 dB per 0.1 nH of bond-wire inductance, while with a magnetic transformer it is just 0.05 dB per 0.1 nH. The minimization of $L_{\rm bond}$ is necessary for achieving high output power with an autotransformer balun.

V. EXPERIMENTAL RESULTS

The bonded die photograph of the fabricated amplifier with an autotransformer balun is demonstrated in Fig. 22. The chip size is 1650 μm × 1000 μm including pads. The design must have been fitted into a predefined size grid, which was larger than needed for the amplifier layout. That is why two quite long lines connecting the input transformer with the bonding pads are

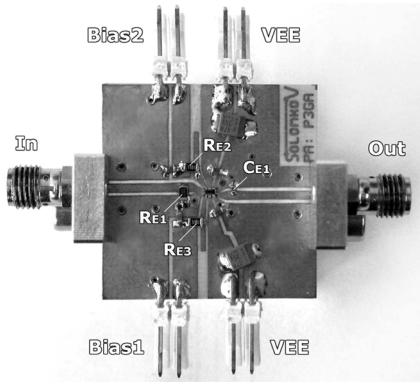

Fig. 23. Test board photograph.

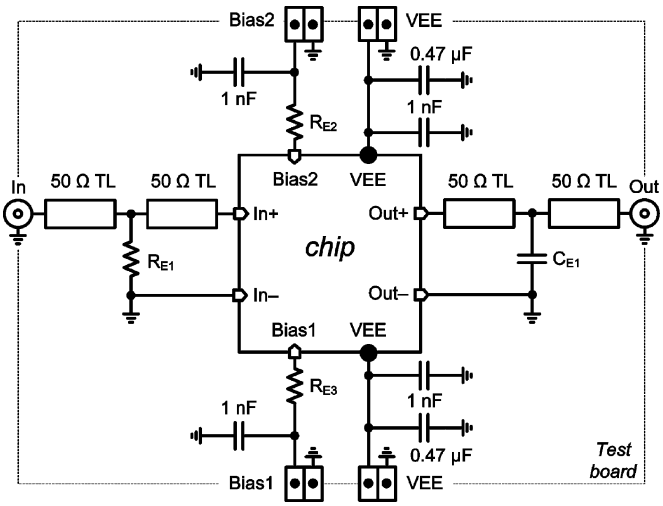

Fig. 24. Schematic of the test board.

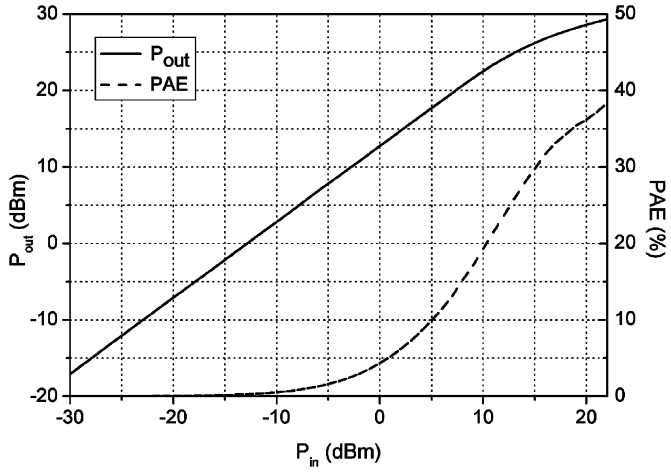

Fig. 25. Measured power transfer characteristic of the PA at 3.5 GHz.

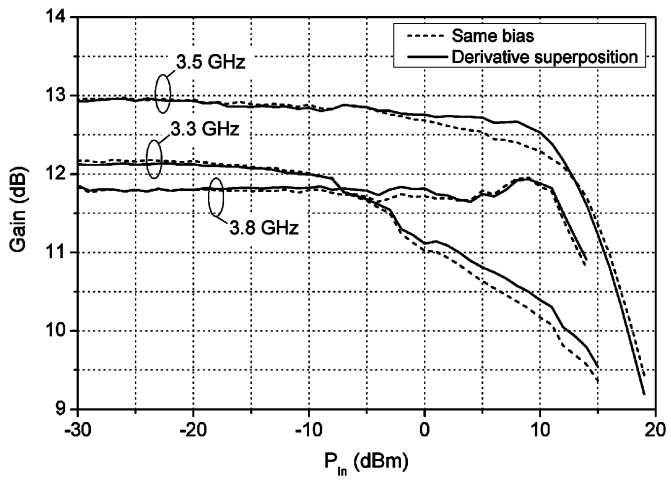

Fig. 26. Measured power gain versus input power.

clearly visible in the photograph. The influence of these lines was taken into account while designing the amplifier.

A. Test Setup

The chip was mounted on a printed circuit board (PCB) employing 50-Ω transmission lines for the input and output signals. In order to minimize bond-wire inductive parasitics, supply pads of the chip were made 390-μm long, which is enough to fit as many as seven 25-μm-wide bond wires (see Fig. 22). The resultant series inductance at "VEE" and "Out-" is approximately 0.15 nH.

Figs. 23 and 24 show a photograph and schematic of the test board. Bias voltages are applied to the chip via resistors R_{E2} and R_{E3} connected in series to the terminals "Bias1" and "Bias2." The value of both resistors is 5.1 kΩ. Capacitor $C_{E1} = 1$ pF matches the output for the best power performance.

Resistor $R_{E1} = 220\ \Omega$ connected in parallel to the input stabilizes the amplifier and prevents the oscillation. At frequencies of around 1 GHz, transistors of the SiGe : C technology used for chip fabrication have significant current gain and the quality factor of passive structures is still high. As a result, the gain of the amplifier at the vicinity of 1 GHz is very high, which is a subject of unwanted oscillations at this frequency. With -1 dB gain penalty, resistor R_{E1} stabilizes the amplifier. A better solution would be to implement a low-loss on-chip feedback compensation network able to suppress the gain at frequencies outside the band of interest. This will become a scope of further implementations.

B. Measurement Results

In all measurements, it is considered that the PA was measured in pulse mode with a pulsewidth of 2 ms and duty cycle of 10% and with an enabled derivative superposition technique, unless otherwise stated. The supply voltage for all measurements was -3.3 V.

The obtained power transfer characteristic at 3.5 GHz is demonstrated in Fig. 25. The amplifier delivers saturated output power of 29.3 dBm at 22-dBm input. The corresponding PAE is 38.8%.

Fig. 26 shows the gain of the amplifier versus input power. In small signal mode at 3.5 GHz, the PA provides 13 dB of gain. 1-dB gain compression occurs at $P_{\rm in} = 12.5$ dBm (corresponding $P_{\rm out} = 24.6$ dBm). The gain curve of the PA when transistors of both differential pairs are biased at the same operating point is drawn in Fig. 26. The derivative superposition technique demonstrates better linearity, offering 0.25 dB higher gain at the edge of the saturation region. The small-signal gain

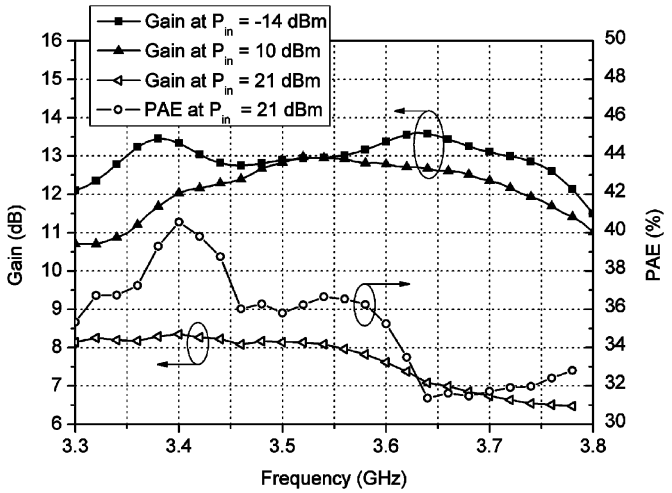

Fig. 27. Measured frequency response of the amplifier.

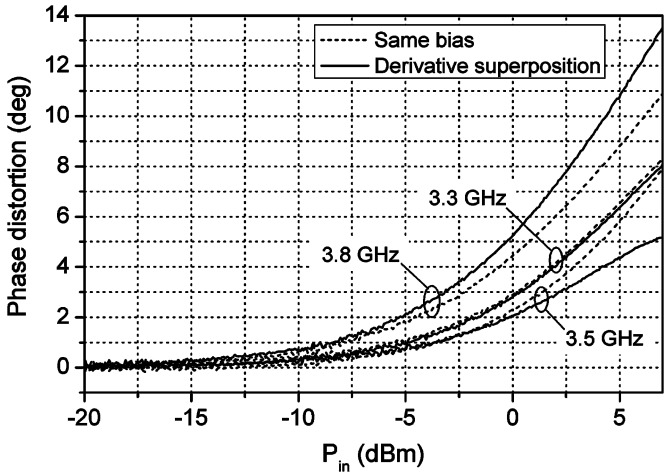

Fig. 28. Measured AM-to-PM response.

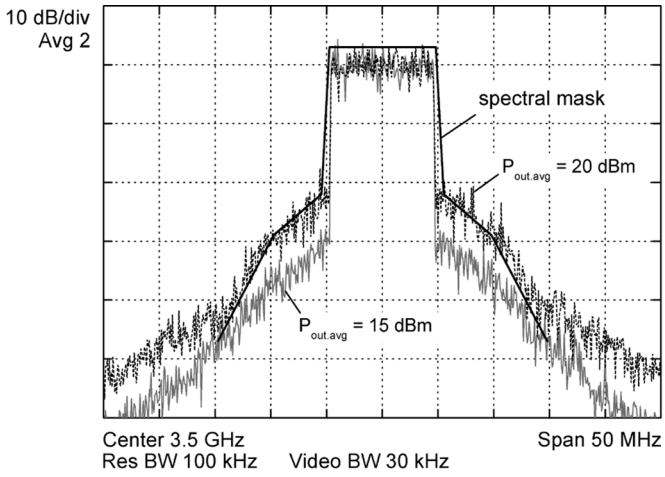

Fig. 29. Measured output spectrum of the PA with OFDM signal (relative power levels are considered).

TABLE II
MEASURED ACPR

$P_{out.avg}$, dBm	ACPR, dBc					
	3.3 GHz		3.5 GHz		3.8 GHz	
	same bias	super-position	same bias	super-position	same bias	super-position
20	–28.6	–29.4	–27.2	–26.5	–28	–28.3
19	–29	–29.7	–28.7	–28.7	–30.3	–30.2
18	–29	–29.8	–29.5	–31	–31.8	–31.5
17	–28.8	–29.8	–30.1	–32.4	–32.2	–31.8
16	–28.8	–29.8	–30.5	–33.4	–32.2	–31.6
15	–28.8	–30.1	–30.9	–34.5	–31.8	–31.4
14	–28.8	–30.1	–31.2	–34.7	–31.7	–31.3
13	–29.2	–30.2	–31.8	–35.4	–31.6	–31.4
12	–29.4	–30.3	–32.4	–35.7	–31.7	–31.5

at the band edges is approximately 1 dB lower. The biasing for enabling derivative superposition at 3.3 and 3.8 GHz is different from that used for 3.5 GHz. At 3.3 GHz, the gain curve exhibits the rolloff already starting from the input power of −5 dBm. The derivative superposition technique compensates the gain compression by 0.2 dB at high drive levels.

Fig. 27 demonstrates the frequency response of the PA. The measurements are performed for different input power settings: −14 dBm (small-signal regime), 10 dBm (moderate nonlinear regime), and 21 dBm (saturation). The gain ripple within the target frequency band for any input power does not exceed 2.2 dB. The PAE of the saturated amplifier goes above 40% at 3.4 GHz.

Phase distortion is measured as a deviation of $\angle S_{21}$ over the input power (see Fig. 28). At 3.5 GHz, the PA with the enabled derivative superposition technique offers the lowest phase deviation from the phase in the small-signal mode. At 3.8 and 3.3 GHz, the derivative superposition does not reduce AM-to-PM distortions. This can be improved at the expense of gain degradation at high drive levels.

AM-to-AM and AM-to-PM responses (Figs. 26 and 28) already give a lot of information about the linearity of the PA. Using these characteristics, the analytical prediction of error vector magnitude (EVM) or adjacent channel power ratio (ACPR) specifications for an orthogonal frequency division multiplexing (OFDM) PA is possible [10]. However, they do not provide any information about the gain deviation within the desired and adjacent channels and memory effects in power transistors. To verify properly the amplifier's linearity, it was tested with a 1024-point fast Fourier transform (FFT) OFDM signal defined in 802.16-2004 [11]. An Agilent E4438C vector signal generator was used to generate the channel signal with the following parameters: 3.5-GHz center frequency, 10-MHz bandwidth, data bursts using 64 quadrature amplitude modulation (64-QAM) modulation type. The average channel power applied to the PA was 3 and 8 dBm. The obtained power spectrum of the output signals of the PA, as well as the transmit spectral mask specified in [11], are demonstrated in Fig. 29. As is recommended in [11], the resolution and video bandwidth were set to 100 and 30 kHz, respectively. The PA was measured in continuous wave (CW) mode.

For corresponding input signals, the PA delivered the average power of 15 and 20 dBm, which is 9.6 and 4.6 dB below the 1-dB compression point, respectively. Nonlinearities of the amplifier contribute to power emission outside the main channel. The PA output signal is covered by the specified spectral mask up to the average output power of 15 dBm. In order to achieve

23-dBm transmission typical for the WiMAX mobile station, power combining of several amplifiers is necessary because a further increase of output power will result in intolerable nonlinear distortions.

In order to demonstrate the improvement in linearity offered by the derivative superposition technique, the measured ACPR at the center band and band edges for different biasing configurations are demonstrated in Table II. Here, ACPR is defined as the ratio between the total power of the adjacent channel measured in the 10-MHz bandwidth to the main channel's power. The adjacent channel is 10 MHz away from the center frequency of the main channel. The PA with an enabled derivative superposition technique has superior ACPR over a major portion of the WiMAX band. The power emission into the adjacent channel just at 3.8 GHz is slightly higher than in the case when all transistors are biased to the same operating point. The maximum allowed ACPR can be calculated from the transmit spectral mask and is equal to -30.3 dBc.

VI. Discussions and Conclusion

The presented PA demonstrates a fairly linear power transfer response over a major portion of the 3.3–3.8-GHz WiMAX band and state-of-art saturated PAE (the reader is referred to [12] and [13] for other push–pull PA designs for 3.5-GHz WiMAX). Such result was achieved due to the derivative superposition method implemented in the active part and integrated autotransformer balun. The obstacle to achieving better linearity at band edges is a narrowband output matching network, which will become a scope of improvements in future design iterations.

Solid theoretical analysis and simulations of the autotransformer balun prove that it offers lower power losses than the conventional transformer balun. The major disadvantage of the autotransformer when using it as a balanced-to-unbalanced converter is the asymmetry introduced into the push–pull amplifier, resulting in a common mode bounce of an on-chip ground. From this perspective, the PA comprising the autotransformer balun can be treated as an alternative between the single-ended and push–pull architecture. It is not as sensitive to the parasitic ground inductance as a single-ended amplifier, but still more sensitive than a PA with the magnetic transformer balun. Therefore, the minimization of the common mode supply inductance is necessary for achieving high performance.

It was illustrated that the degree of asymmetry is the higher, the lower is the coupling between the specific windings in the autotransformer. By taking this into account, one can conclude that the efficient usage of the autotransformer balun is possible only at low-gigahertz frequencies. Already at 5 GHz the autotransformer becomes compact in order to operate below the self-resonance frequency, which results in a poor coupling factor. Moreover, at very high frequencies, the common mode ac signal that appeared due to some asymmetry introduced by the balun can essentially degrade the gain and delivered power.

In future implementations, the driver stage should be added to the amplifier, which we believe will not essentially change the efficiency. The possibility of using a power-combining structure should be investigated in order to achieve a target channel power of 23 dBm for WiMAX mobile stations.

Acknowledgment

The authors are grateful to W. Bakalski, Infineon Technologies, Munich, Germany, for many helpful discussions and suggestions.

References

[1] A. Vasylyev, P. Weger, W. Bakalski, and W. Simbürger, "Fully integrated 32 dBm, 1.5–2.9 GHz SiGe-bipolar power amplifier using power-combining transformer," *Electron. Lett.*, vol. 41, no. 16, pp. 908–909, Aug. 2005.

[2] D. Webster, J. Scott, and D. Haigh, "Control of circuit distortion by the derivative superposition method," *IEEE Microw. Guided Wave Lett.*, vol. 6, no. 3, pp. 123–125, Mar. 1996.

[3] S. C. Cripps, *RF Power Amplifiers for Wireless Communications*, 2nd ed. London, U.K.: Artech House, 2006.

[4] I. Bahl, *Lumped Elements for RF and Microwave Circuits*. London, U.K.: Artech House, 2003.

[5] P. M. Jupp and D. R. Webster, "Application of derivative superposition to low IM3 distortion IF amplifiers," in *RF Circuit Technol. Workshop*, Cambridge, U.K., Mar. 2002, pp. 9–16.

[6] Y.-S. Lee, M.-W. Lee, and Y.-H. Jeong, "Linearity-optimized 3.5 GHz GaN HEMT Doherty amplifier," in *23rd Int. Circuits/Syst., Comput., Commun. Tech. Conf.*, Jun. 2008, pp. 1065–1068.

[7] C. Lu, A.-V. H. Pham, M. Shaw, and C. Saint, "Linearization of CMOS broadband power amplifiers through combined multigated transistors and capacitance compensation," *IEEE Trans. Microw. Theory Tech.*, vol. 33, no. 3, pp. 2320–2328, Nov. 2007.

[8] J. McRory and R. Johnston, "Self-bias for class B bipolar transistors," in *Can. Elect. Comput. Eng. Conf.*, May 1996, pp. 855–858.

[9] I. Bahl, "Low loss matching (LLM) design technique for power amplifiers," *IEEE Microw. Mag.*, vol. 5, no. 4, pp. 66–71, Dec. 2004.

[10] R. Marŝálek, "Analytical EVM calculation for OFDM systems with nonlinear power amplifiers," in *Proc. Student EEICT Conf.*, 2003, pp. 115–119.

[11] *IEEE Standard for Local and Metropolitan Area Networks-Part 16: Air Interface for Fixed Broadband Wireless Access Systems*, IEEE Standard 802.16-2004, Oct. 2004.

[12] B. Jin, Q. Wu, G. Yang, F. Meng, J. Fu, and K. Tang, "Fully integrated CMOS power amplifier design for WiMAX application with semi-lumped transformer," in *6th IEEE Int. Ind. Inform. Conf.*, Jul. 2008, pp. 181–185.

[13] T. Wooten and L. Larson, "A decade bandwidth, low voltage, medium power class B push–pull Si/SiGe HBT power amplifier employing through-wafer vias," in *Radio Freq. Integr. Circuits Symp.*, Jun. 2008, pp. 519–522.

Valentyn A. Solomko was born in Kyiv, Ukraine, in 1982. He received the B.S. and M.S. degrees (with honors) from the National Technical University of Ukraine, Kyiv, Ukraine, in 2003 and 2005, respectively, and the Ph.D. degree (*summa cum laude*) in electrical engineering from the Brandenburg University of Technology, Cottbus, Germany, in 2008.

He is currently a Scientific Assistant with the Chair of Circuit Design, Brandenburg University of Technology. His research interests focus on design and measurement of microwave analog and mixed-signal integrated circuits.

Peter Weger was born in South Tyrol, Italy, in 1958. He received the M.S. degree in theoretical physics from the University of Innsbruck, Innsbruck, Austria, in 1984, and the Ph.D. degree in electronics from the Technical University of Vienna, Vienna, Austria, in 1991.

From 1984 to 1998, he was a Member of Technical Staff with Siemens Corporate Research, Munich, Germany. He has been involved in a variety of projects related to high-speed logic (Si bipolar), gigabit electronics (10 Gb/s), and circuits (single-chip transceivers, PAs) for wireless communication. Since 1998, he has held the Chair of Circuit Design with the Brandenburg University of Technology, Cottbus, Germany.